DWH NRDA Marine Mammal Technical Working Group Report: Assessing the Likelihood of Dolphin Carcass Strandings in the Northern Gulf of Mexico

Damrongsak Wirasaet, Jessica D. Meixner and Joannes J. Westerink

Department of Civil and Environmental Engineering and Earth Sciences
University of Notre Dame, Notre Dame, IN, 46545

September 2, 2015

1 Introduction

This work uses Lagrangian particle tracking in an assessment of the observed bottlenose dolphin carcass standings in the Northern Gulf of Mexico during and after the Deepwater Horizon oil spill. The primary objective was to identify the likely origin of carcasses that were discovered between Galveston Bay and Mobile Bay from June 2010 to June 2011 (Figure 1). If the origin can be estimated then one may be able to identify the dolphin stock component from which the carcass arose. Further, by examining the fate of other particles from the area occupied by the originating stock component, an estimate of the number of carcasses that were not recovered can be secured.

Given a velocity field, Lagrangian particle tracking is a way to estimate the trajectory of individual particles that could represent any number of objects ([1, 2, 3, 4]). This method requires a good representation of the velocity field. Since most dolphin carcasses were discovered in nearshore areas, the currents used in transporting particles (i.e., virtual dolphin carcasses) need to represent nearshore circulation in an area that is geometrically complex. The only way to get such a velocity field in the study area is to use a high resolution numerical circulation model. In this work, we use the currents from the high-resolution ADCIRC (ADvanced CIRCculation) model [5]. Due to the use of an unstructured mesh and its high-scalability on parallel computing platforms, ADCIRC is capable of handling multi-scale problems from basin scale phenomena, to inlet scale flows, to feature scale flows such as flow around jetty. The spatial resolution of the mesh or grid used for hydrodynamic calculations is as fine as 20-30m in the nearshore and intra-tidal zones. This assessment deploys a large number of virtual carcasses uniformly over large areas of a modeled representation of the northern Gulf of Mexico and tracks their positions over defined periods of time.

In the case of tracking dolphin carcases, a number of issues arise. The changes in the buoyancy of dolphin carcasses with respect to size and condition are not well established and could be important. For instance, when fully submerged, it is reasonable to assume that carcasses are transported purely by hydrodynamic currents. But when partially submerged, wave-induced drift and wind-induced drag also contribute to the movement of the carcasses. The influence of winds on floating objects in general is not currently an exact science and search and rescue operations often use a range of possible relationships in practice. As shall be discussed below in Section 2, we explored the search and rescue literature and

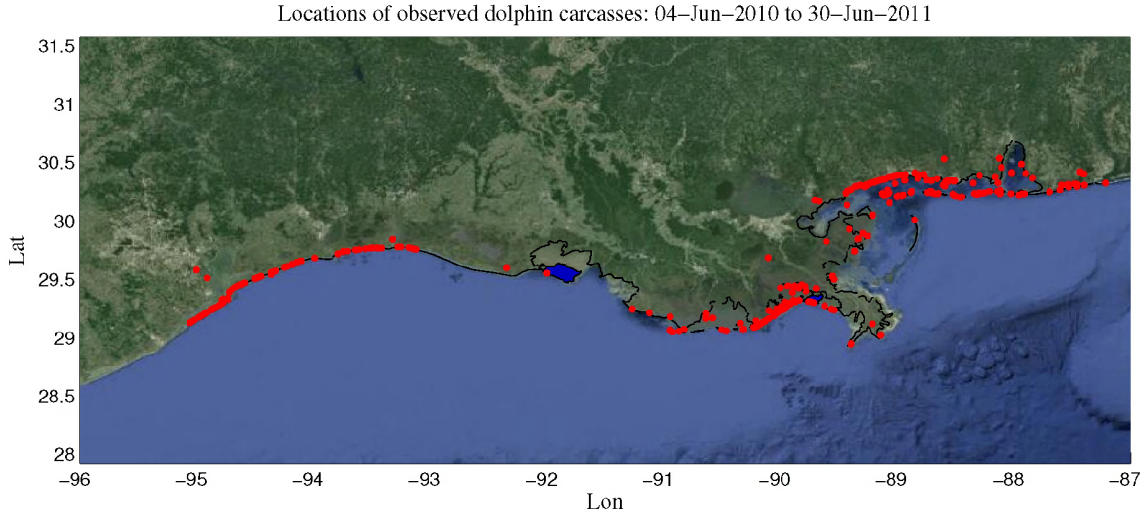

Figure 1: Locations of dolphin carcasses observed from June 2010 to June 2011 (source: NOAA-Fisheries, SEFSC). Black lines represent the area designated as the stranding areas in the model result.

use a fractional wind exposure approach to account for the effect of wind-induced drags when particles simulating dolphin carcasses are exposed to the wind.

The remainder of the report is organized as follows. In Section 2, we describe in detail the methodologies used in this study. The subsequent section (Section 3) contains results from this assessment, including the distribution of stranded carcasses and their likely origins. Conclusions from the study are drawn in Section 4.

2 Methodology

2.1 Lagrangian particle tracking

The trajectory of an individual particle representing a dolphin carcass is computed by integrating

$$\frac{d\boldsymbol{x}(t;\boldsymbol{x}^0)}{dt} = \boldsymbol{u}(\boldsymbol{x}(t;\boldsymbol{x}^0),t), \quad \boldsymbol{x}(t=0) = \boldsymbol{x}^0 \tag{1}$$

where $\mathbf{u}$ is a particle velocity and $\boldsymbol{x}^0$ is the original position of the particle. An object partially immersed in the water surface is transported not only by the water current but also by wind and waves. The latter two may cause the trajectory of the object to deviate from that driven by water currents alone. To account for these effects, we adopt a simple, widely-used approach that considers the combination of the currents $\boldsymbol{u}_c$ and the object velocity relative to the currents, $\boldsymbol{u}_l$, as the particle velocity, more specifically

$$\boldsymbol{u} = \boldsymbol{u}_c + \boldsymbol{u}_l. \tag{2}$$

We derive the currents $\boldsymbol{u}_c$ from the hindcasts of the continental shelf/estuarine hydrodynamic circulation in the Gulf of Mexico for the time period of April 2010 to June 2011 using the high-resolution hydrodynamic ADCIRC model. The model, based on the unstructured-mesh finite element method,

represents estuaries and wetlands, the continental shelf, and the deep Gulf of Mexico in high resolution. The model uses the so-called SL16 mesh which has mesh resolution as fine as 20-30m in the nearshore and intra-tidal zones [6]. Winds, tides, atmospheric pressure, Coriolis, and rivers are the primary forces that drive the flow in the hindcasts; realistic data from both models and observations of these forcings are utilized in the calculations. A detailed account and comprehensive performance evaluation of the hindcasts can be found in [7]. In the tracking calculations, we use a 30-minute time resolution of the currents (note that a significantly smaller time step is used in the hydrodynamic simulations themselves).

It is noted that several model assumptions needed to be accepted to conduct this work. The hindcasts exclude the effect of wind-induced waves, which is arguably an important process of very nearshore circulation. Currents obtained from the ADCIRC model are depth-averaged currents and vertical structure in the velocity field could be important. The model is barotropic and baroclinic processes related to the presence of freshwater are not captured. Since the model is based on the barotropic assumption and run in a two dimensional mode, the model currents become less physically realistic as one moves seaward toward the shelf break and the open Gulf of Mexico. However, ADCIRC has an excellent performance record in the study region, and it was the only circulation model capable of providing such a high resolution representation of the geometrically complex and large study area. Because the model does include river discharge into the model domain, some aspects related to this volume flux are represented. Furthermore, the model was extensively validated in [7] and model currents match relatively well with the observed currents measured at near-shore locations which was the primary focal region for the project. We discuss below the relative velocity $\boldsymbol{u}_l$ which is also refered to as the drift velocity.

2.1.1 Relative velocity

After reviewing the available literature, we relied largely on drift properties used in the field of oil-spill modeling and operational search and rescue modeling to inform our approach for modeling dolphin carcass drift. The carcasses found in the Gulf of Mexico during this period varied in size from small neonatal dolphins to adults, and we used this information to presume that dolphin carcasses are relatively small in size (i.e., in comparison to typical waves) and partially submerged. For objects of length scale significantly smaller than the length of a wave, it is known that the drift induced by waves is insignificant [8, 9]. This allowed us to simplify and ignore wave-induced effects, and an analysis of a simple setting considering the balance of wind-induced and current-induced drags exerted on a partially submerged object was undertaken (details are in Appendix A). This analysis indicated that relative velocity $\boldsymbol{u}_l$ is linearly proportional to the wind velocity with the coefficient (multiplying the wind) depending on an immersion ratio. The analysis suggested a level of wind fraction that is within the range employed in previous studies in the oil-spill and operational search and rescue modeling.

In oil-spill applications, the relative velocity $\boldsymbol{u}_l$ is commonly taken to be

$$\boldsymbol{u}_l = F_w \mathbf{A} \boldsymbol{u}_w, \quad \mathbf{A} = \begin{bmatrix} \cos\theta & -\sin\theta \\ \sin\theta & \cos\theta \end{bmatrix} \tag{3}$$

where F_w is a constant multiplier, $\boldsymbol{u}_w$ denotes the wind velocity (usually, 10-m height winds), and θ is the deflection angle (positive counter-clockwise) from the wind direction to account for the Ekman effect. The value of F_w is often assumed to be in the range of 0.03-0.035 of 10-m winds in the absence of explicitly derived water currents [10, 11]; the deflection angle, positive for the northern hemisphere, ranges from 3° to 28° as reported in the literature (see e.g. [12, 13, 14]). Dietrich et al. [11] found from their numerical experiments that a 7° wind deflection angle provides reasonable results for surface oil transport patterns in the northern Gulf of Mexico.

In the field of operational search and rescue modeling, a relationship between the relative velocity, also known as the leeway drift, and the 10-m wind speed is determined empirically by field experiments as a way to tackle the very difficult problem of determining the net force on small objects with complex geometries [15, 9, 16, 17]. Note that these analyses explicitly account for water currents. More recently, Breivik et al. [17] describe a more refined procedure, the so-called leeway field method, in collecting and condensing leeway data in a field experiment. The leeway field method condenses the relationship between the downwind component u_{dw} and crosswind leeway component u_{cw} of the leeway drift (the former is the component parallel to the 10-m wind direction and the latter is the component normal to the 10-m wind direction) and the 10-m wind through a set of coefficients arising from the linear regression

$$
\begin{aligned}
u_{dw} &= a_d w_{10} + b_d + \varepsilon_d, \\
u_{cw+} &= a_{cw+} w_{10} + b_{cw+} + \varepsilon_{cw+}, \\
u_{cw-} &= a_{cw-} w_{10} + b_{cw-} + \varepsilon_{cw-}.
\end{aligned}
$$

The observed downwind (right, left crosswind) leeway drift u_{dw} (u_{cw+},u_{cw-}) is related to the 10-m wind speed through the multiplier a_d (a_{cw+},a_{cw-}), the offset b_d (b_{cw+},b_{cw-}), and the Gaussian error term ε_d (ε_{cw+},ε_{cw-}). In the same work, the authors provide the results from the field studies conducted along the Norwegian coast of three objects, namely a medium-sized shipping container (~3.6m×0.7m×0.8m), a 55-gallon oil drum (cylinder with a diameter of 58 cm and a length of 87 cm), and a WW-II mine (oval shape of 125 cm in height and 105 cm in diameter). The immersion ratio of these objects ranges approximately from 60% to 70%. The results show that the downwind leeway drift range approximately from 0.008 (the oil drum) to 0.02 (the mine) of the 10-m wind speed. Among these objects, only the oil drum exhibits significant crosswind leeway drift of approximately 0.004-0.006 of the wind speed.

The above mentioned previous works reflect the use of a wide range of wind percentages and deflection angles in Lagrangian tracking of drifting objects. Since we are dealing with both partially submerged objects (presumably) similar in size and submersion ratio as those studied by Breivik et al. [17] and we explicitly compute water currents, we are inclined to use the leeway drift approach and the results of their field studies, i.e. with wind percentages of approximately less than 2%. In addition, this level of wind percentage is also supported by the simple estimate we derived in Appendix A (although the analysis is simplistic at best) which suggests a wind percentage of approximately 1.6% for an object with 60% immersion ratio and with a 50cm-height above the surface water. Note that in our tracking simulations that consider the wind-driven drift, the value of the drift velocity is calculated from the 10-m North American Mesoscale (NAM) wind product[1], which are also the winds used in the hydrodynamic model runs.

2.1.2 Remarks on particle tracking algorithm

Given the initial location, the trajectory of each particle is obtained by numerically integrating equation (1) using a 4^{th}-order Runge-Kutta time stepping scheme with an adaptive time step size to control error in the integration. More precisely, the time step is chosen based on the error determined by comparing the position of the particle at time $t + \delta t$ when integrating with the time step δt and with the time step $\delta t/2$. If the error is greater than the given tolerance, the time step is cut in half and re-integrated until the determined error is less than the tolerance. Note that, with sufficiently small error tolerance in the time integration, the resulting time step size would also ensure that the particle would cross only one element at the end of each time marching step. The time marching procedure requires the value of velocity (current and wind) at the particle location. Here, this value is obtained from the linear interpolation in time and space of the nodal data given on the finite element mesh. The particle is not allowed to cross a levee or a land boundary. If a new position of the particle crosses such a boundary, the

[1]NAM winds can be obtained at `http://nomads.ncdc.noaa.gov/data/namanl/`

particle position is instead set to a location on the boundary and subsequently determined by tracking along edges. In a tracking task with direct wind, the contribution of wind to the particle velocity is set to zero if the particle location resides in an element adjacent to land or a levee to prevent the wind contribution from artificially transporting the particle across the levee or land boundaries.

2.2 Initial seeding and tracking period

In this study, we tracked a large number (approx. 11 million) of particles that are initially near-evenly distributed over a large area spanning the coastal areas and the continental shelves of Louisiana, Mississippi, and Alabama as a means of assessing the stranding of marine carcasses. The initial seeding areas are enclosed in the polygons shown in Figure 2. The initial seeding was carried out in two steps.

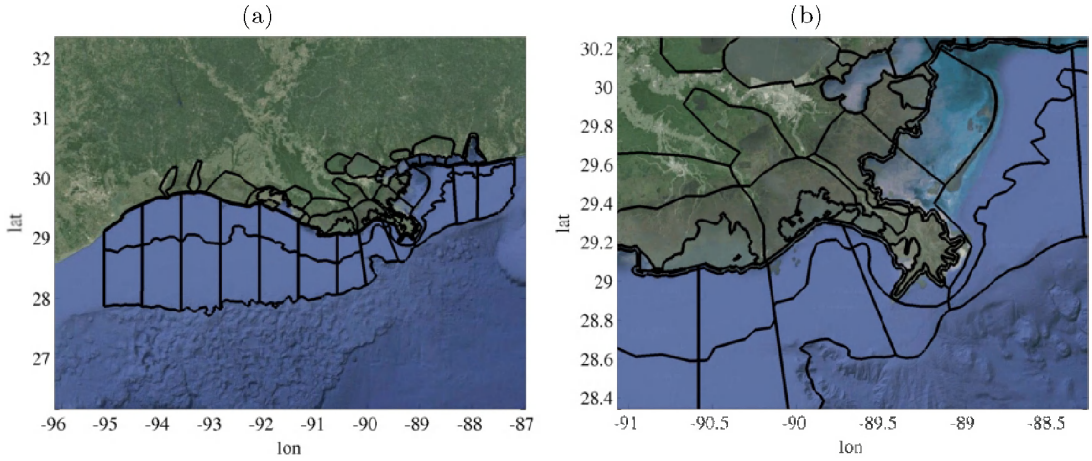

Figure 2: (a) Polygons enclosing the initial seeding areas; (b) seeding areas in South-Eastern Louisiana.

First, 10^6 particles per square degree of longitude and latitude were scattered over each polygon. Second, particles in locations where the water depth is shallower than 80 cm were removed. This resulted in tracking a pool of approximately 11 million seeded particles. This set of seeded particles is released every 7 days over a period of one year with the first set being released on June 1, 2010 and the last set on June 14, 2011. For each release, each individual particle is tracked for 15 days.

We consider two scenarios in the tracking: (i) particles transported only by water currents (driven by atmospheric pressure, winds, tides, and riverine discharge) and (ii) particles transported by currents and the 1% wind drift with a 7° deflection angle. It is noted that the magnitude of wind ranges from the same order to two orders of magnitude greater than the current speed; thus the 1% wind drift ranges from a small fraction of the current speed to a contribution as large as the current itself. Therefore, one could expect discernible differences between results from these two scenarios.

2.3 Assessment and stranding zones

Lagrangian tracking provides a time series of individual particle locations for the entire period of tracking. The particle tracking thus furnishes information that may be used in examining the final distribution of particles (i.e., virtual carcasses) originating from different sites of interest. This allows us to locate where particular carcass, stranded at a certain location and time, was likely to have

originated from. It allows us to explore to where other particles from that same general area (i.e., stock component area) were likely transported.

In these analyses, once the particles enter pre-identified stranding zones, they are declared *stranded*, i.e. their positions are unchanged thereafter[2]. The stranding zones represent an area with a possibility of dolphin carcasses to wash up on. Here, the probable stranded zones of interest include beaches, thin coastal strips, and islands along the northern Gulf Coast from East of Galveston, TX to Mobile Bay, AL (see Figure 3(a) for an illustration of polygons representing the defined stranding zones).

2.4 Transition matrix

One of the products of this work is the so-called *connectivity* or *transition* matrices. The connectivity matrix has been employed widely in marine population studies (see [18] and references therein) to systematically examine the exchange of particles between different sites. An entry (i, j) of the transition matrix $\mathbf{N}(t; t_0)$ represents the population or the proportion of the population, when normalized with the number of particles, originating from the i^{th} site at t_0 to reach the j^{th} site after a $t - t_0$ tracking period. In other words, the i^{th} row of the matrix contains the information of the particle population that, at time t, reaches different zones from the i^{th} zone; the j^{th} column of the matrix indicates the population from different zones that constitute the population of the j^{th} zones at time t. When a scenario of stranding is considered, the entry (i, j) of the transition matrix, with the j^{th}-zone being a stranding zone, is the cumulative population, originating from the i^{th} zone, that are stranded in the j^{th} zone. Note that we can compute the transition matrices both with and without the terminal stranding consideration discussed above.

The reported transition matrices are built based on the set of polygons[3] illustrated in Figure 2. There are a total of 190 polygons in this set. These polygons represent areas that can be grouped roughly as follows: probable stranding zones which consist of beaches (88 polygons) and islands (24 polygons) dotted along the shoreline; inner-coastal water zones (18 polygons) buffering the stranding zones and deeper water zones; bays (6 polygons); inland water zones including lakes and marsh areas (21 polygons); deltas (1 polygons) and sounds (8 polygons); outer-coastal zones (12 polygons) buffering inner-coastal zones and continental-shelf zones; continental-shelf zones (12 polygons). Figure 3 depicts zones based on the above simplified classification.

Note that the entries in the transition matrix related to a starting location associated with a stock component and a stranding zone (e.g., beaches, islands) are a primary output. These values represent the probability that a particle (i.e., virtual carcass) from a given stock will strand in a particular stranding zone. This is the *probability of beaching* described in [19].

3 Results

3.1 Distribution of stranded particles and their origins

Before discussing results of the model strandings, we show, as an example in Figures 4 and 5, the particle positions after their release. These figures depict the results from the current tracking model and the current-wind tracking model, respectively. The release time of these particles is June 1, 2010.

[2] In the actual tracking, the stranded participles are allowed to be transported further; we simply discard the trajectories after the time at which they become stranded in the analysis step.

[3] This set of polygons, based loosely on a set of crude polygons we introduced, were carefully devised by Lance Garrison of NOAA Fisheries.

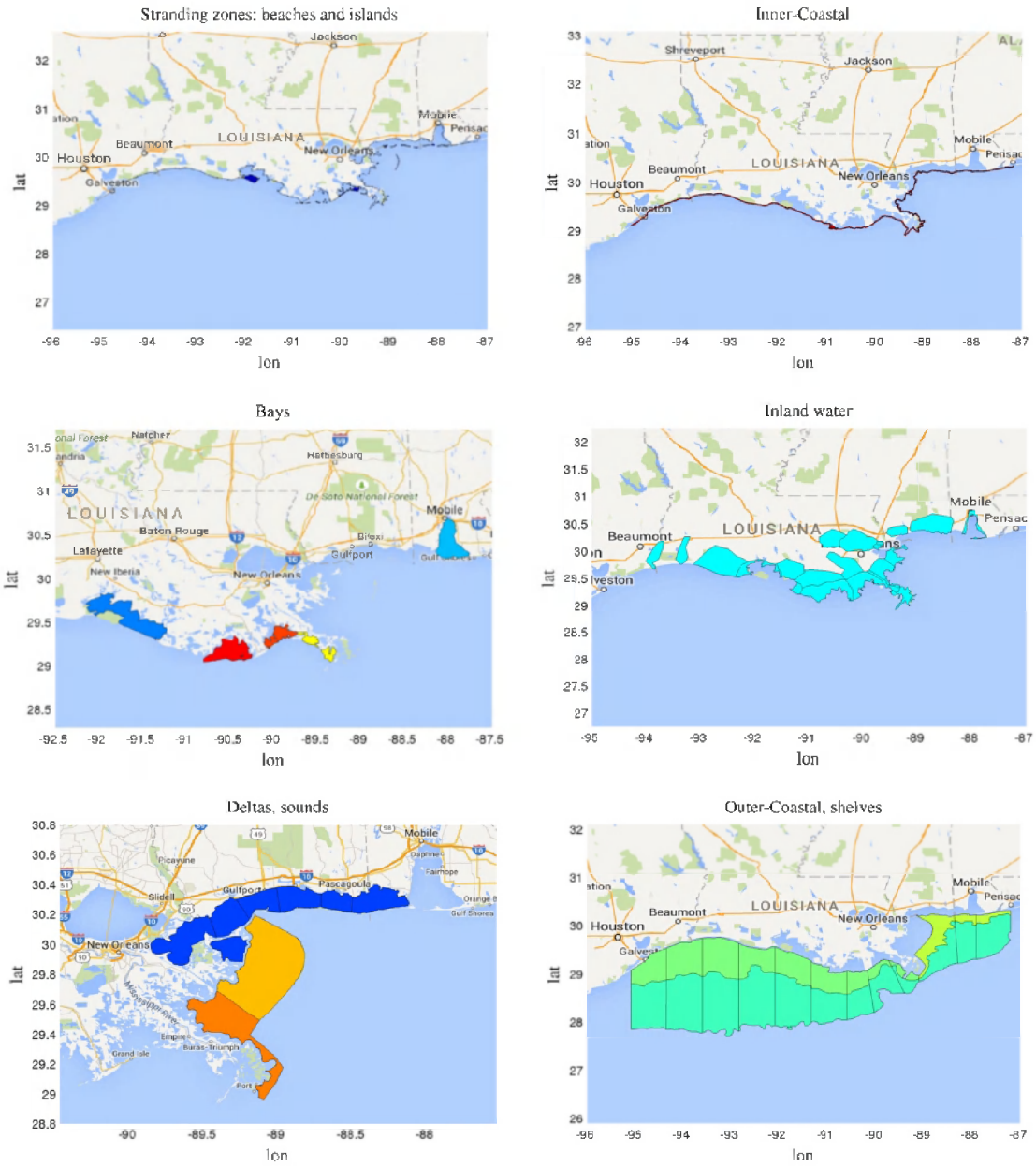

Figure 3: Classification of zones. From top and left to right: probable stranding zones; inner coastal zones; bays; inland coastal water zones; delta and sounds; outer- coastal zones and continental shelves.

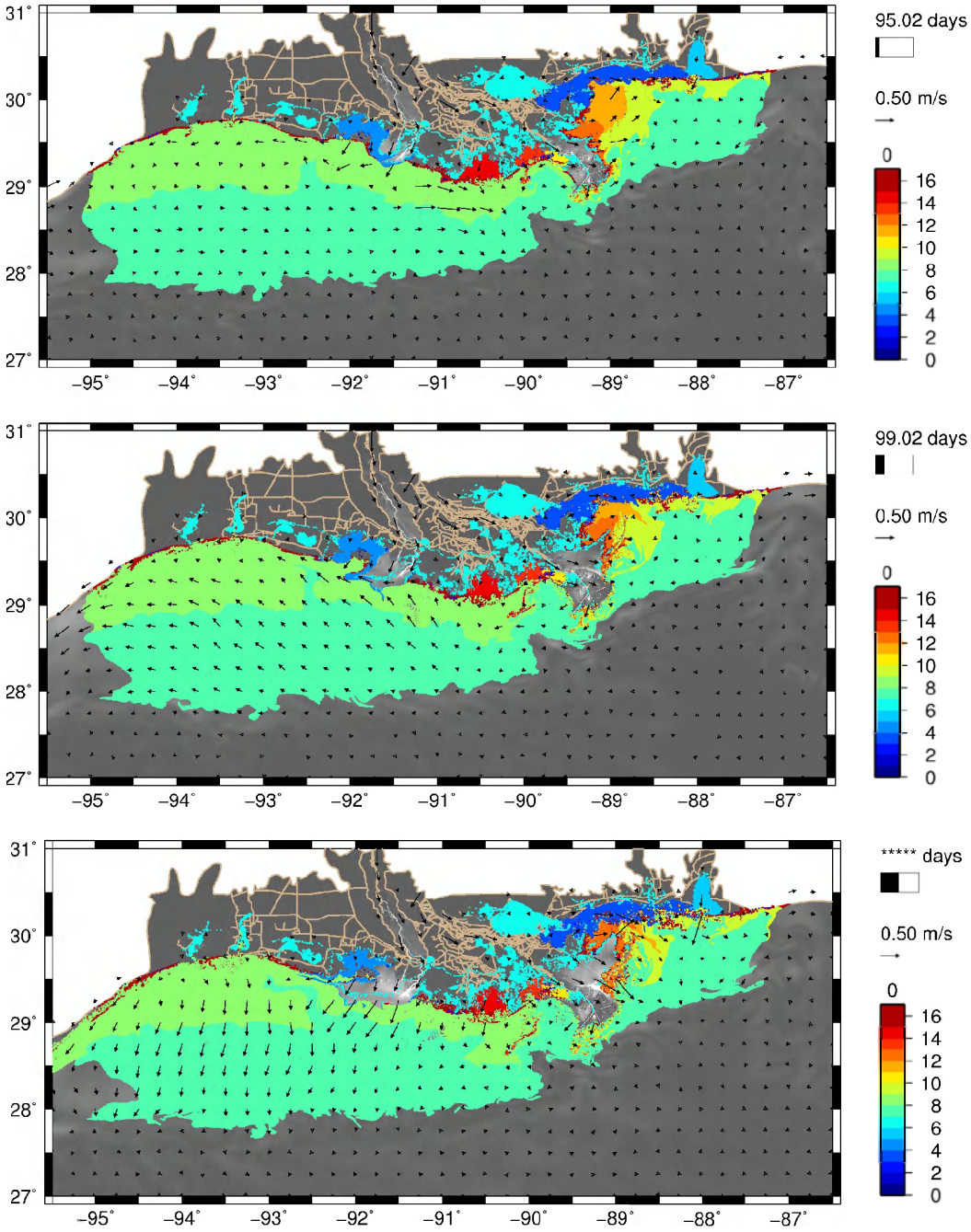

Figure 4: Positions of particles after initial release for the *current only* tracking model. Top: 3 days after release, middle: 5 days, bottom: 7 days. Initial release time: 06/01/2010. Color represents orginal release area. The shift in the spatial distribution of the color is due to advection of particles by water currents only.

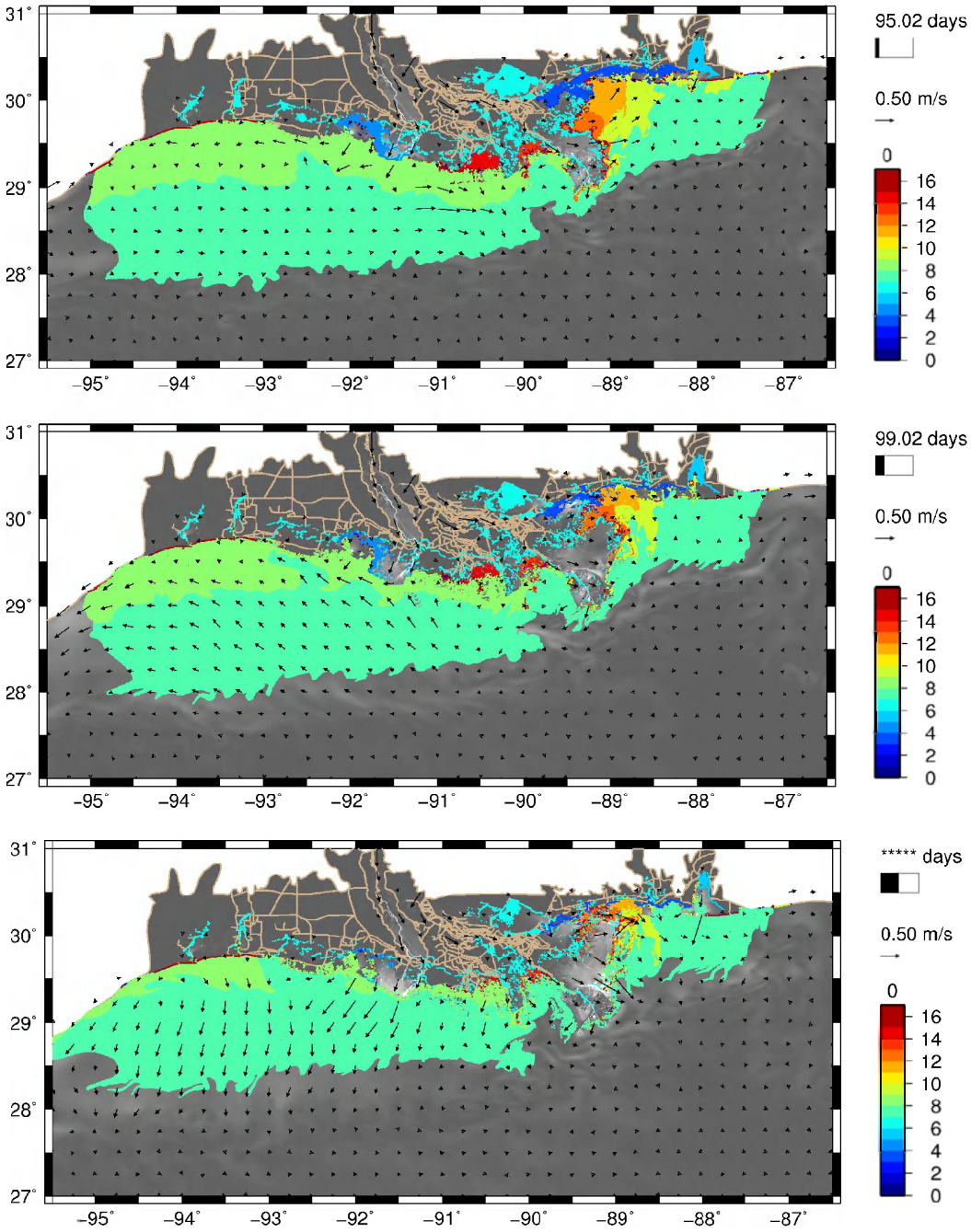

Figure 5: Positions of particles after initial release for the *current-wind* tracking model. Top: 3 days after release, middle: 5 days, bottom: 7 days. Initial release time: 06/01/2010. Color represents orginal release area. The shift in the spatial distribution of the color is due to advection of particles by water currents and wind.

In these figures, each particle is assigned a color representing the zone in which it was originally released; the color scheme of the release zones is illustrated in Figure 2. The change in the spatial distribution of a color through time is caused by the transport of particles by water currents or the combination of water currents and wind. In addition, we use a grayscale to depict the velocity magnitude (the lighter, the higher current velocity) and use arrows to represent the current magnitude and direction. The distinct differences between the two simulations can be clearly discerned from these plots. It appears that the current-wind tracking model moves more particles from the deeper areas to the shallower areas than the current only tracking model. In addition, the current-wind tracking model appears to pin particles in inland lakes against their shores. In both models, the particles in the vicinity of the Mississippi Delta or the so-called "Birds Foot" and Atchafalaya Delta appear to be transported away from those regions. This is clearly due to riverine driven outward currents.

Next, we examine the data pertaining to the positions of stranding particles at 3, 5, 7 days prior to the time they are declared stranded to gain a better idea on the sources and the source's strength of the stranded particles. We simply divide a box enclosing the release polygons into a set of uniform $N_x \times N_y$ cells and determine points belonging to each cell. This allows us to use the density (the number of the particles per area of a cell) as an indicator of the level of the source strength. Figures 6 and 7 show the source density of the particles using the current only tracking model and the current-wind tracking model, respectively.

In Figures 6 and 7, the plot in the top row shows the areas covering the positions at 3, 5, and 7 days before stranding of the stranded particles from all releases; the plots in the remaining rows depict an average source strength. Note that, in the area plots, the areas covering the origins at 3, 5, and 7 days prior to stranding are colored in order from dark to pale shades.

It can be observed from Figure 6 that, for the current-only tracking model, the eventually-stranded particles generally originate from areas in close proximity to the stranding zones. Duration of drift (i.e., 3, 5, and 7 days) does not impact this interpretation greatly, especially in the areas along the Texas Coast. In the current-wind tracking model, the source positions cover areas extending approximately 0.5° to 1° ($\sim$ 25-100 km) from the shore lines. Furthermore, distinct differences can be clearly discerned in the extent of the particle positions at 3, 5, and 7 days before strandings. In Figure 8, we fill the regions between contour levels[4] of the averaged source strength of the current-wind tracking model. The contour levels displayed in the plots are those values given in a colorbar to the right of each plot.

It can be clearly observed from this figure that the density of the origins of the stranding particles is inversely proportional to the distance from the shores, *i.e.* high concentration near shore and low concentration in areas further away from the shore. In addition, it can be seen that the areas with relatively high particle density ($> (40/7.27) \times 10^5$) separate roughly into four areas: (i) Mississippi Sound and Chandeleur Sound, (ii) the areas including Bays and shores east of the Bird Foot, (iii) areas west of the Atchafalaya Delta, and (ii) and an area along the Texas coast roughly west of the outlet of Sabine Lake. These areas appear to be separated by major deltas or major outlets. In addition, the origin concentration is relatively low around the Bird foot, especially to the west, and the area immediately off the Atchafalaya Delta.

It is noted that the above analysis simply gives an idea of the most likely areas that stranded particles arise from in an average sense. The analysis effectively averages out event-scale variability in winds and currents over the simulation year. This is a partial picture and similar analyses focused on a single month demonstrate that the source areas for stranded particles does in fact vary to various degrees, from relatively mild to substantial, from the results shown above.

[4]The fill color corresponds to that of the lower contour level

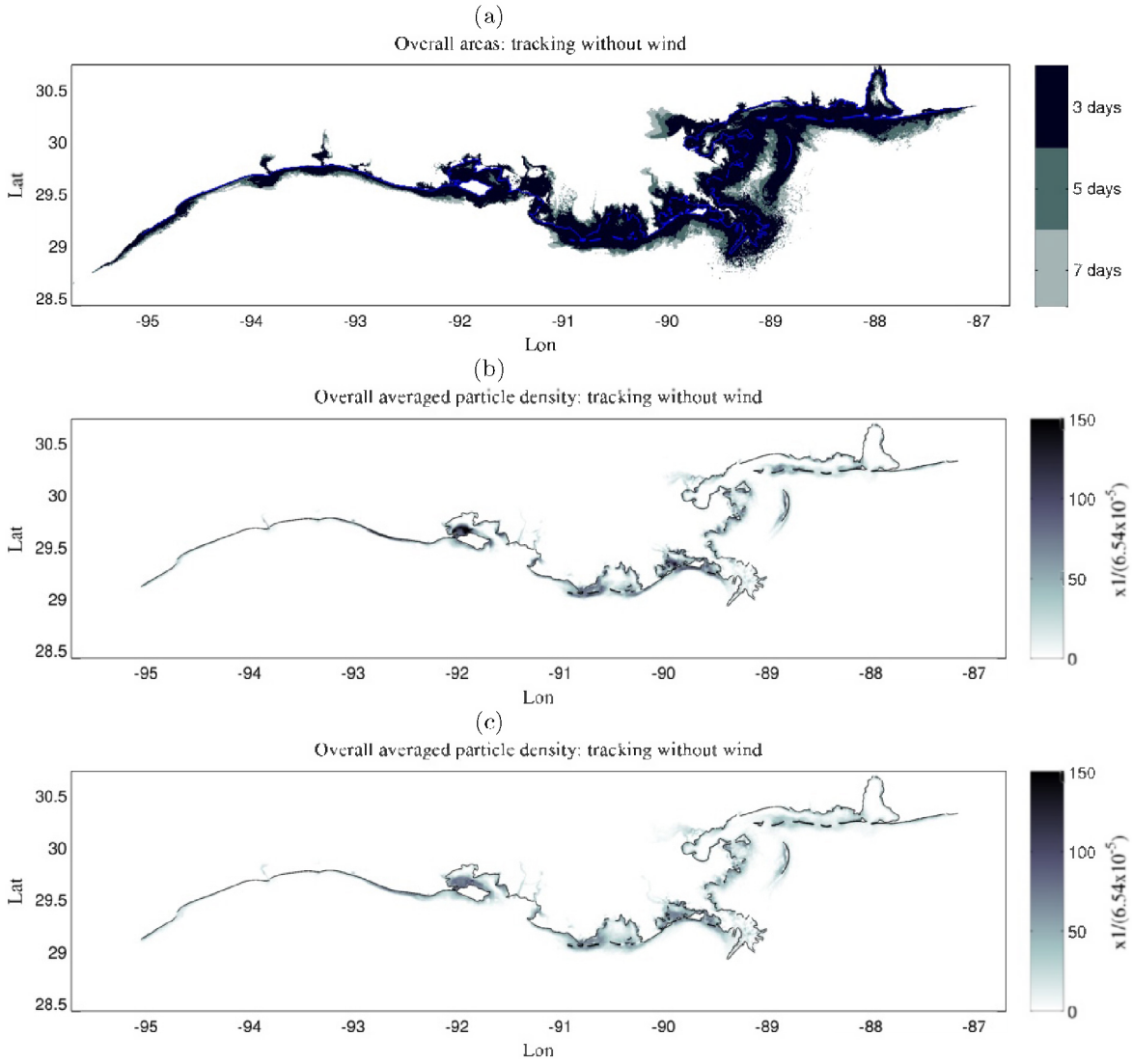

Figure 6: Extent and strength of source locations of the current only tracking model. (a) Overall areas covering the positions of eventually-stranded particles at 3, 5, and 7 days prior to being stranded (the areas covering the origins at 3, 5, and 7 days prior to stranding are colored in order from dark to pale shades); (b), (c) Average source strength (points per area) associated with the locations of the eventually-stranded particles at (b) 3 days and (c) 7 day prior to being stranded.

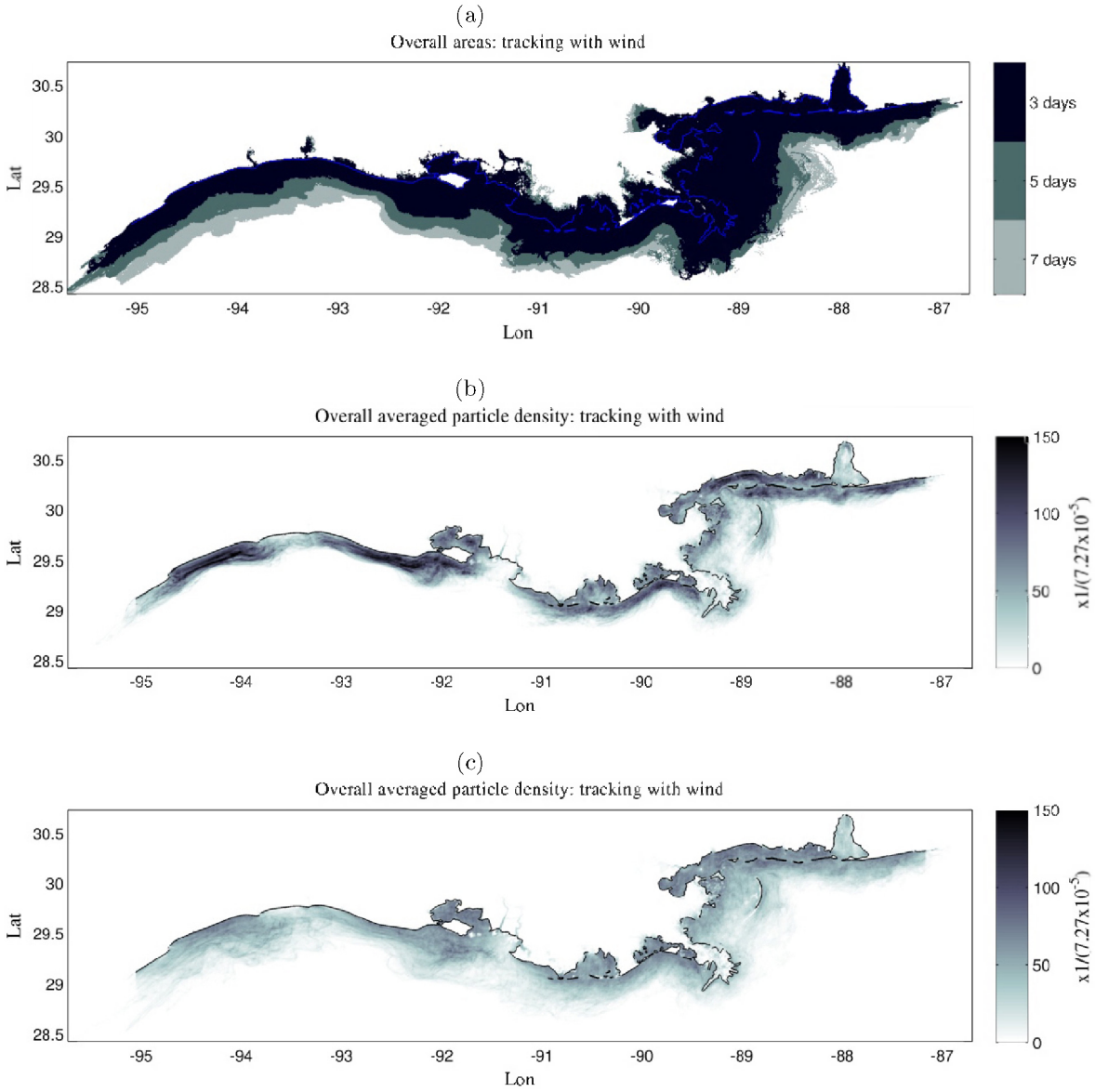

Figure 7: Extent and strength of source locations of the current-wind tracking model. (a) Overall areas covering the positions of eventually-stranded particles at 3, 5, and 7 days prior to being stranded (the areas covering the origins at 3, 5, and 7 days prior to stranding are colored in order from dark to pale shades); (b), (c) Average source strength (points per area) associated with the locations of the eventually-stranded particles at (b) 3 days and (c) 7 day prior to being stranded.

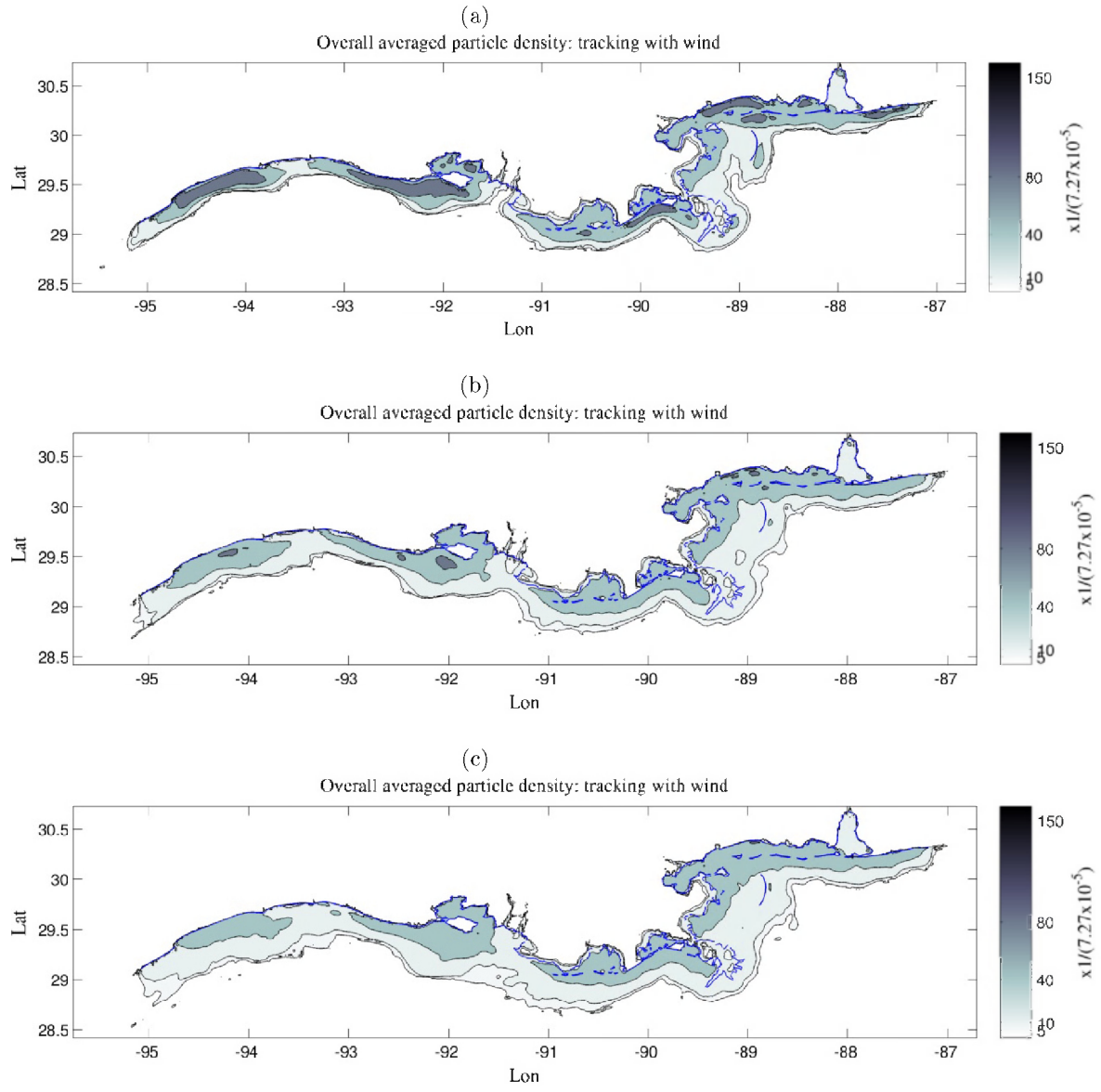

Figure 8: Current-wind tracking model. Source strength associated with the particles locations at (a) 3, (b) 5, and (c) 7 days prior to being stranded. Regions between the contour levels are filled with the color of the lower contour level.

3.2 Assessing the origins of observed carcasses from tracking model

Here, we use the model results to estimate the areas from which each observed carcass might have originated. To accomplish this task, for the specific location and time that each observed carcass was found, we locate the particles for each tracking release that land in the proximity of both the carcass's location (and in the same stranding zone to which the observed carcass belongs) and the time when the observed carcass was first sighted. We subsequently extract, from their trajectory, the positions of these particles before they are declared stranded. Results shown below, unless otherwise indicated, are obtained by considering the particles that land within 750-m radius of the carcass location and become stranded at the time that falls within 24hr before and 12hr after the observed stranding time. In addition, the results shown below are those derived from the current-wind tracking model.

Figure 9 shows the trajectories and positions of particles that are stranded in the location and time proximity of each dolphin carcass found in each week of February 2011 (see Appendix B for the results associated with the observed carcasses found in other months).

In these plots, red, dark orange, and light purple squares respectively indicate the locations where the virtual carcasses are stranded and the positions of the particle at 3 days and 7 days prior to their stranding time[5]. The carcasses for which there is no virtual particle landing in their proximity are marked by the green diamonds in these plots. Figure 10 shows an enlarged view of the trajectories of the virtual carcasses that are stranded in the proximity of four dolphin carcass found in the Barataria Bay area during the week of 02/15/2011-02/22/2011. In this figure, the green circles are used to mark the locations of the observed carcasses, which lies on top of a cluster of red squares depicting the stranding locations. The dark orange and light purple squares indicate the particle location 3 and 7 days prior to stranding while the magenta lines indicate the particle trajectories.

Figure 11 shows the results of a specific carcass *68IMMS070510* found on 02/19/2011. In this Figure, the location of this carcass is marked by the red circle. We show the positions of the virtual carcasses at 3 days and 7 days before becoming stranded in the carcass's proximity with the purple squares. In addition, we show enclosures of areas in which these positions are relatively densely clustered. Note that the enclosures for the positions at 3 days and 7 days are colored with yellow and green colors, respectively. It is noted that since the particles are released every week and each release is tracked for 15 days, the particles stranding in the proximity of the observed carcass come from one to three different releases. It can be clearly noticed that the particles landing in the proximity of the observed carcasses are, to a large extent, local, *i.e.* they come from nearby areas with displacement distance less than 0.5° to 1° away (however, the length along the trajectories in general are generally longer than the displacements between the origins and the stranded locations).

4 Conclusions

Passive Lagrangian particle tracking models are used in assessing the the observed strandings in the Northern Gulf of Mexico for the time period from June 2010 to June 2011. The models use wind-driven currents from the high-resolution ADCIRC hindcasts and 10m-NAM winds. Two scenarios are considered in tracking: (i) virtual carcasses transported only by currents and (ii) virtual carcasses transported by water currents and 1% winds and a 7° deflection angle. The former represents the scenario where the virtual carcasses are fully submerged and the latter when partially submerged. The wind percentage is used to account for wind-induced drags and the 1% fraction is guided by the simple

[5]To be more precisely, in Figure 9, if the particles become stranded from day 0 to day 3 after the release, their origins are marked by the dark orange squares; if the particles become stranded from day 3 to day 7 after the release, their origins are marked by the light purple squares.

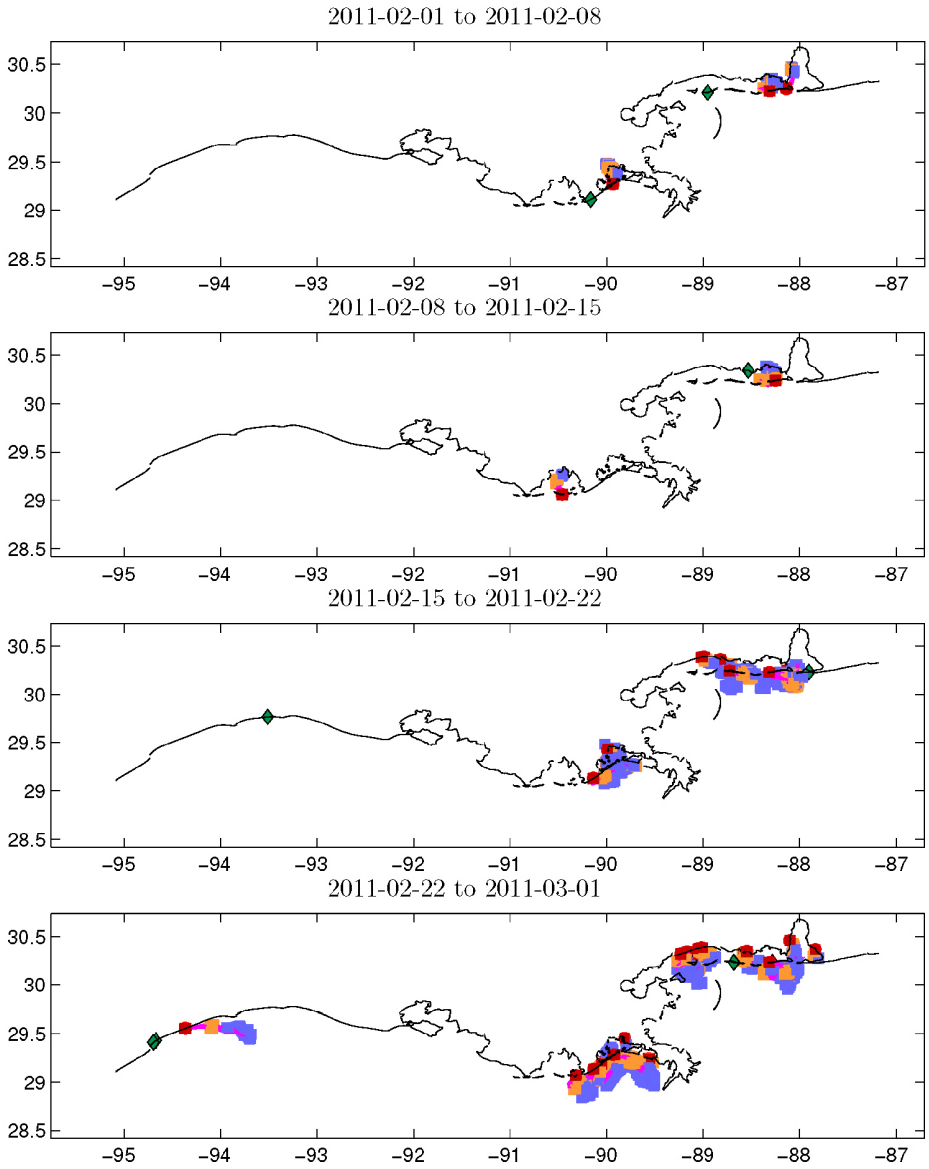

Figure 9: Current-wind tracking model. Origins, stranding locations, and trajectories of virtual carcasses landing in the proximity, both in time and location, of each observed carcass sighted in each week of Feb 2011. Magenta lines represents trajectories; red, dark orange, and light purple square symbols the stranding positions, the locations 3-day before stranding, and 7 days before stranded, respectively. A green diamond symbol marks the location of an observed carcass in which no virtual carcass is stranded in its proximity.

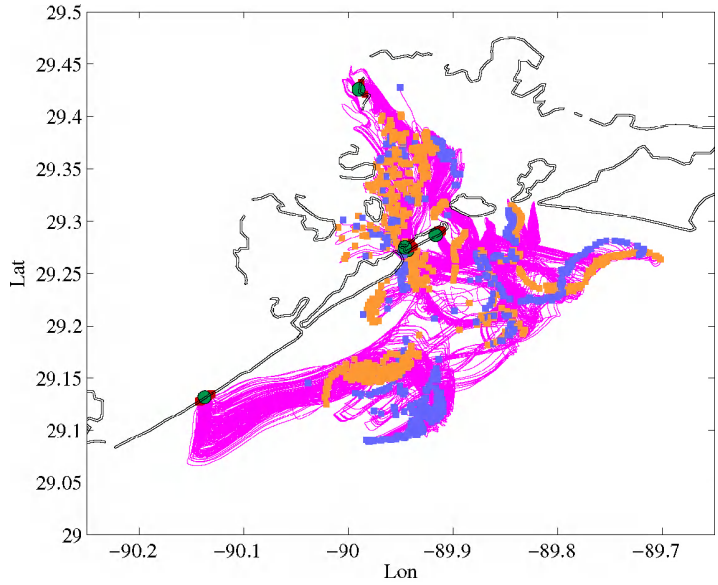

Figure 10: Current-wind tracking model. Trajectories and positions of particles landing in the proximity of each observed carcass sighted during 02/15/2011-02/22/2011 in Baratraria bay. Description for symbols are identical with those for Figure 9. The green circles are used to marked the locations of the observed carcasses.

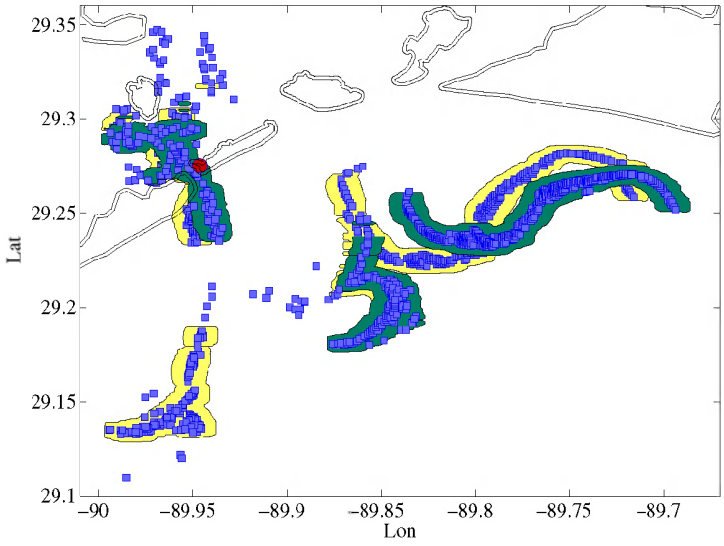

Figure 11: Current-wind tracking model. Areas covering the origins of particles stranded in the proximity of the carcass *68IMMS070510* found on 02/19/2011. The red circle is the location of the carcass. Green and yellow colored areas cover the positions of virtual carcasses 3 days and 7 days (including those stranding in between 3 to 7 days if the stranding happened before 7 days after the release time) prior to stranding, respectively.

estimate based on the balance of wind-induced and current-induced drags for 60% submergence as well as from previous field experiments.

In the assessment, we use a large number of virtual carcasses seeded uniformly over large areas. The assessment consists of collecting strandings, which are the virtual carcasses entering the areas designated as the stranding zones, and examining their trajectories before being declared as strandings. Examining the origins of the strandings reveals that the origin positions of the model strandings cover areas extending approximately less than 0.5° to 1° (25-100 km) from the shorelines. In these coverage areas, the origins of stranded particles are clustered in areas nearshore and scattered away from the shore. In addition, the density of stranding origins is relatively low around the major deltas, to the west of the Bird foot, and the area immediately off the Atchafalaya Delta. Close examination of the origins of the virtual carcasses landing in both location and time proximity of the observed carcasses clearly show that the virtual strandings, to a large extent, local, *i.e.* originate from the nearby areas and are likely associated with proximal dolphin stock components.

In this work, the 1% wind fraction used here is guided by analysis and field experiments. It is a reasonable estimate but certainly not a precise nor complete account of the effect of the wind-induced drift. This term should be varied with time due to the changes in shape, composition, and submergence factor of the dolphin carcass. To gain more confidence in the assessment, the use of other wind fractions or varying wind fractions may be considered; a number of tracking scenarios exhibiting good correlations of the strandings is subsequently used in locating the likelihood of where the strandings might have come from.

5 Acknowledgements

We thank John Quinlan and Lance Garrison of NOAA Fisheries for their generosity in providing us data, input, and feedback.

Appendix

A Estimating wind factor

It is found in previous studies (see [9, 17] and references therein) that the drift speed rapidly approaches its terminal velocity and the stationary solution may be applied to good approximation. We use this finding in a simplified estimate of the wind effect on a partially immersed object. In the estimate, the winds and currents are assumed steady and the forces acting on the protruding and submerged portions of the object obey the quadratic drag law. For simplicity, we show an analysis for a 1-D setting (see Figure 12 for a schematic diagram of the problem). Note the analysis below can be extended directly to a similar 2-D setting. Here, let A_a, A_w denote the areas of the object that are exposed to air and submerged in water, respectively and W, V, U denote the wind, current, and (to-be-determined) object's velocity, respectively. By selecting a reference frame that travels with the object, a balance of wind and water induced drags can be written as

$$\frac{\rho_a A_a C_a}{2}(\widetilde{W}+V_L)^2\frac{(\widetilde{W}+V_L)}{|\widetilde{W}+V_L|}+\frac{\rho_w A_w C_w}{2}(V_L)^2\frac{V_L}{|V_L|}=0$$

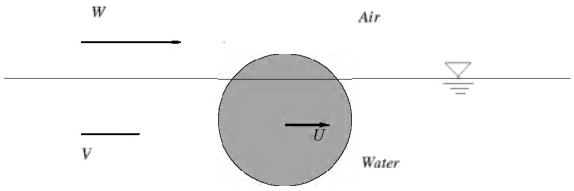

Figure 12: Schematic diagram describing the problem of a partially-submerged drifting object

where $\widetilde{W} = W - V$ and $V_L = V - U$. The signs of $\widetilde{W} + V_L$ and V_L must be opposite in order for a solution to exist. It is sufficient to consider only the case where V_L is negative and $\widetilde{W} + V_L$ is positive; in this case, one has

$$r(\widetilde{W} - \widetilde{V}_L)^2 = \widetilde{V}_L^2 \tag{4}$$

where $\widetilde{V}_L = |V_L|$ and

$$r = \frac{\rho_a A_a C_a}{\rho_w A_w C_w} = \frac{\rho_a C_a}{\rho_w C_w} \left(\frac{A}{A_w} - 1 \right), \tag{5}$$

where $A = A_a + A_w$ is the total area and A/A_w is the inversion of the immersion ratio. The solution $\widetilde{V}_L$ of (4) is determined by

$$\frac{\widetilde{V}_L}{\widetilde{W}} = \frac{r - r^{1/2}}{r - 1} = \frac{r^{1/2}}{r^{1/2} + 1}. \tag{6}$$

Equation (6) implies that $V_L = V - U$, the so-called leeway drift, is linearly proportional to the magnitude of of the wind velocity (not the magnitude squared). Figure 13 plots the ratio $\widetilde{V}_L/\widetilde{W}$ as a function of the ratio of the total area and submersed area A/A_w (here, we use $\rho_a = 1.125$ and $\rho_w = 1000$ kg/m^3 and assume that $C_a = C_w$). Note that the formula above is based on winds near surface. The

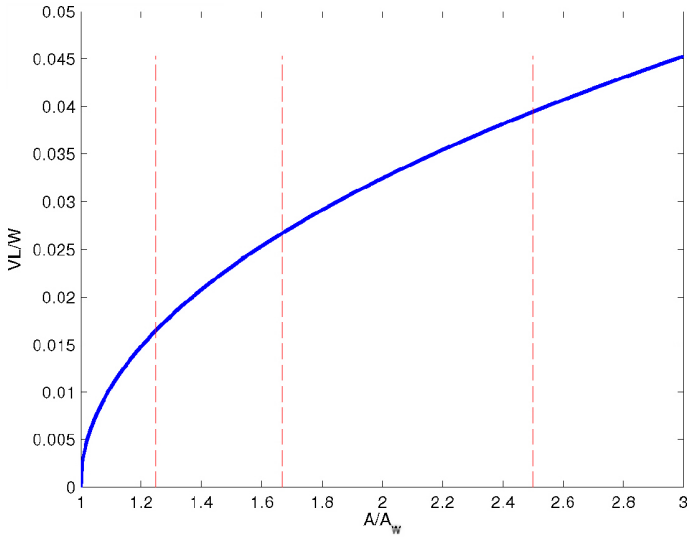

Figure 13: The ratio of leeway drift V_L and $\widetilde{W} = W - V$ as a function the ratio of the total area and submersed area A/A_w. Red vertical lines mark from left to right mark the ratio leeway drift ratio for the object with an 80%, 60%, and 40% submersion ratio, respectively.

logarithmic wind profile can be employed in determining wind at a certain height from 10-m wind data which is typically used in circulation models. The logarithmic wind profile (see [20]) is given by

$$u_z = \frac{u_*}{\kappa}\left[\ln\left(\frac{z-d}{z_0}\right)\right]$$

where u_* is the friction velocity, κ is the Von Karman constant (-0.41), d is the zero displacement, z_0 is the surface roughness. Given 10-meter winds, the wind velocity at a given height is determined by

$$w = w_{10}\frac{\ln(z-d)-\ln(z_0)}{\ln(10-d)-\ln(z_0)}$$

For open water, $z_0 = 0.0002$ and d is taken to be $\frac{2}{3}z_0$. Figure 14 shows the wind profile with respect to 10-m wind. A vertically-averaged velocity at $z = H$ is given by

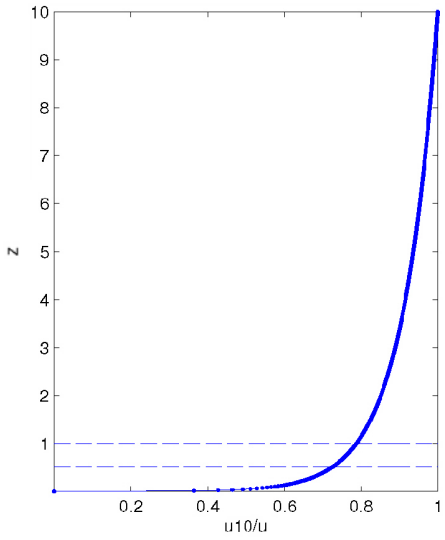

Figure 14: w_z/w_{10} as a function of height above the water surface

$$\begin{aligned}\overline{w} &= \frac{w_{10}}{\widetilde{H}\left[\ln(10-d)-\ln(z_0)\right]}\left[\int_{d+z_0}^{H}\ln(z-d)dz-\ln(z_0)\right] \\ &= w_{10}\left[\frac{\{(H-d)\ln(H-d)-(H-d)-z_0\ln z_0+z_0\}}{\widetilde{H}[\ln(10-d)-\ln(z_0)]}-\ln(z_0)\right] \qquad (7)\end{aligned}$$

where $\widetilde{H} = H-d-z_0$. Table (1) tabulates vertically-averaged wind speed with respect to the 10-m wind at a various height. Formula (7) can then be used in (6) for an estimate based on 10-m winds. As an example, from these analysis (7 and 6), the drift velocity of an object which is 60% submerged and protrudes 50 cm from surface water is approximately 0.026*(0.6310*$W_{10}-U$) $\sim 0.016W_{10}$ (approximately $\sim$ 1.6% of the 10-m wind velocity for $W_{10} \gg U$).

Table 1: $\frac{\overline{w}}{w_{10}}$ at various heights H above the sea surface.

H	$\overline{w}/w_{10}$
0.125	0.5034
0.25	0.5671
0.50	0.6310
0.75	0.6684
1.00	0.6949

References

[1] Quinlan, Blanton, Miller, and Werner. From spawning grounds to the estuary: Using linked individual-based and hydrodynamic models to interpret patterns and processes in the oceanic phase of Atlantic menhaden Brevoortia tyrannus life history. *Fisheries Oceanography*, 8:224–246, 1999.

[2] M.R. Larson, M.G.G. Foreman, C.D. Levings, and M.R. Tarbotton. Dispersion of discharged ship ballast water in Vancouver Harbour, Juan De Fuca Strait, and offshore of the Washington Coast. *Journal of Environmental Engineering and Science*, 2(3):163–176, 2003.

[3] S. Carniel, G. Umgiesser, M. Sclavo, L.H. Kantha, and S.Monti. Dispersion of discharged ship ballast water in vancouver harbour, juan de fuca strait, and offshore of the washington coast. *Science and Justice*, 42(3):143–151, 2002.

[4] H. Peltier, W. Dabin, P. Daniel, O. Van Canneyt, G. Dorémus, M. Huon, and V. Ridoux. The significance of stranding data as indicators of cetacean populations at sea: Modelling the drift of cetacean carcasses. *Ecological Indicators*, 18:278 – 290, 2012.

[5] R. A. Luettich, Jr, J. J. Westerink, and N. W. Scheffner. ADCIRC: An advanced three-dimensional circulation model for shelves, coasets, and estuaries: Theory and methodology of ADCIRC-2DDI and ADCIRC-3DL. Technical report DRP-92-6, US Army Corps of Engineers, DC, 1992.

[6] J.C. Dietrich, J.J. Westerink, A.B. Kennedy, J.M. Smith, R.E. Jensen, M. Zijlema, L.H. Holthuijsen, C. Dawson, R.A. Luettich Jr., M.D. Powell, V.J. Cardone, A.T. Cox, G.W. Stone, H. Pourtaheri, M.E. Hope, S. Tanaka, L.G. Westerink, H.J. Westerink, and Z. Cobell. Hurricane Gustav (2008) waves and storm surge: Hindcast, synoptic analysis, and validation in Southern Louisiana. *Monthly Weather Review*, 139:2488–2522, 2011.

[7] D. Wirasaet and J.J. Westerink. ADCIRC circulation modeling: Deepwater horizon oil spill in 2010. DWH ATTORNEY WORK PRODUCT/ATTORNEY-CLIENT COMMUNICATIONS Final Report. August, 2014.

[8] J. Grue and D. Biberg. Wave forces on marine structures with small speed in water of restricted depth. *Applied Ocean Research*, 15(3):121 – 135, 1993.

[9] B. Hackett, Ø. Breivik, and C. Wettre. Forecasting the drift of objects and substances in the ocean. In E.P. Chassignet and J. Verron, editors, *Ocean Weather Forecasting*, pages 507–523. Springer Netherlands, 2006.

[10] M. Reed, C. Turner, and A. Odulo. The role of wind and emulsification in modelling oil spill and surface drifter trajectories. *Spill Science & Technology Bulletin*, 1(2):143 – 157, 1994.

[11] J.C. Dietrich, C.J. Trahan, M.T. Howard, J.G. Fleming, R.J. Weaver, S. Tanaka, L. Yu, R.A. Luettich Jr., C.N. Dawson, J.J. Westerink, G. Wells, A. Lu, K. Vega, A. Kubach, K.M. Dresback, R.L. Kolar, C. Kaiser, and R.R. Twilley. Surface trajectories of oil transport along the northern coastline of the Gulf of Mexico. *Continental Shelf Research*, 41:17 – 47, 2012.

[12] T. Audunson. The fate and weathering of surface oil from the bravo blowout. *Marine Environmental Research*, 3(1):35 – 61, 1980.

[13] L. Malcolm, L.S. Eric, Anderson, T. Isaji, and E. Howlett. Simulation of the oil trajectory and fate in the Arabian Gulf from the Mina Al Ahmadi spill. *Marine Environmental Research*, 36(2):79 – 115, 1993.

[14] A.H. Al-Rabeh. Estimating surface oil spill transport due to wind in the Arabian Gulf. *Ocean Engineering*, 21(5):461 – 465, 1994.

[15] A.A. Allen and J.V. Plourde. Review of leeway: field experiments and implementation. Technical report, DTIC Document, 1999.

[16] Ø. Breivik and A.A. Allen. An operational search and rescue model for the Norwegian Sea and the North Sea. *Journal of Marine Systems*, 69(12):99 – 113, 2008. Maritime Rapid Environmental AssessmentNew Trends in Operational Oceanography.

[17] Ø. Breivik, A.A. Allen, C. Maisondieu, and J.C. Roth. Wind-induced drift of objects at sea: The leeway field method. *Applied Ocean Research*, 33(2):100 – 109, 2011.

[18] R.K. Cowen, C.B. Paris, and A. Srinivasan. Scaling of connectivity in marine populations. *Science*, 311(5760):522–527, 2006.

[19] Marine Mammal Injury Quantification Team (MMIQT). Models and Analyses for the Quantification of Injury to Gulf of Mexico Cetaceans from the Deepwater Horizon Oil Spill. *DWH NRDA Marine Mammal Technical Working Group Report*, 2015.

[20] S.D. Smith. Coefficients for sea surface wind stress, heat flux, and wind profiles as a function of wind speed and temperature. *Journal of Geophysical Research*, 93(C12):15467–15472, 1988.